

# Constrained Optimization Based Control of Real Time Large-Scale Systems: Airjet Object Movement System

W. B. Jackson,<sup>a</sup> M. P. J. Fromherz,<sup>b</sup> D. K. Biegelsen,<sup>b</sup> J. Reich,<sup>b</sup> D. Goldberg<sup>b</sup>

<sup>a</sup>HP Labs, 4U-12, 1501 Page Mill Road, Palo Alto, CA 94304 U.S.A.

<sup>b</sup>Xerox PARC, 3333 Coyote Hill Road, Palo Alto, CA 94304, U.S.A.  
warren\_jackson@hp.com

## Abstract

The control of real time, nonlinear, large-scale systems – systems with large aggregations of sensors and actuators – is seldom explored in actual operating physical systems. In such many-element systems, control issues such as actuation allocation, fusion of sensor data, and system identification emerge as challenging problems for large-scale system control. In this work, constrained optimization is used to solve these problems as applied to the control of an object moving system with 1,152 actuators and 32,000 sensors with a 2 ms control loop time. Solutions for allocating actuation among large numbers of actuators using hierarchical constrained optimization and fusing the output of many sensors into a small number of final measurements under tight real time constraints have been developed. This paper demonstrates that hyper-redundant systems are capable of system self-identification – the aggregate of properties of many elements can be used to measure detailed properties of individual elements. This work demonstrates that constrained optimization can effectively solve problems associated with control of many-element systems.

## 1. Introduction

As the cost of control system elements – sensors, actuators, and processors – decreases, systems with large numbers of control elements become increasingly cost competitive with existing systems. For such systems, a control approach that considers the limitations of communication bandwidth and memory of typical low-cost distributed hardware is an important problem.

Usual control methods such as linear system theory can provide theoretical control solutions, but when the number of sensors or actuators becomes large, the sensors or actuators are nonlinear (e.g., binary), and there are a number of constraints, these solutions do not scale well and require significant communication and computational resources if applied in the standard way. Model predictive control (MPC) can handle such large-scale constraint problems [Allgöwer *et al.*, 1999; Bemporad *et al.*, 2000; Bequette, 1991; Rawlings and Muske, 1993] but typically

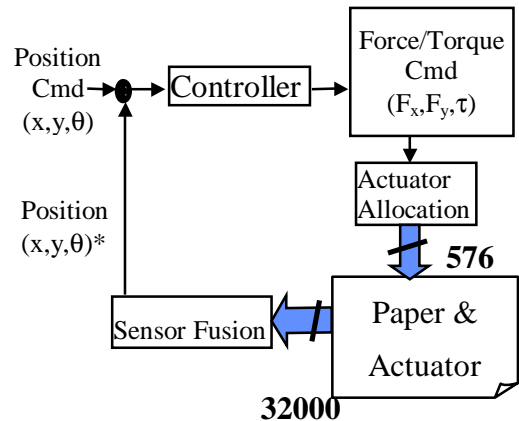


**Figure 1** Control loop for airjet system. The numbers indicate the dimensionality of the signal paths. The blocks indicate the various steps.

has not been applied to real time systems because of the long time required to find solutions.

In this work, we present the use of constrained hierarchical optimization to solve large-scale real time control problems particularly for the solutions of the sensor fusion and actuator allocation problems. These solutions are applied to an actual air-jet object transport system with 1,152 actuators and 32,000 sensors [Berlin *et al.* 2000, Biegelsen *et al.* 2000].

## 2. Theoretical Framework

**State Equation** – The behavior of large-scale systems can be characterized by the state equation

$$\begin{aligned} \frac{d\mathbf{x}}{dt} &= f(\mathbf{x}) + g(\mathbf{x}, \mathbf{u}) + f_{ext}(\mathbf{x}, \mathbf{u}) \\ \mathbf{y} &= h(\mathbf{x}) \end{aligned} \quad (1)$$

where  $\mathbf{x} \in \mathcal{R}^n$  is the state of the system,  $\mathbf{u} \in \mathcal{R}^m$  is the actuation vector of the system,  $\mathbf{y} \in \mathcal{R}^p$  is the state of the sensors,  $f_{ext}(\mathbf{x}, \mathbf{u})$  is an optional applied external force, and  $m, p \gg n$ . We will confine our discussion to large-scale systems with a low-dimensional state space but high-dimensional actuation and observational spaces.

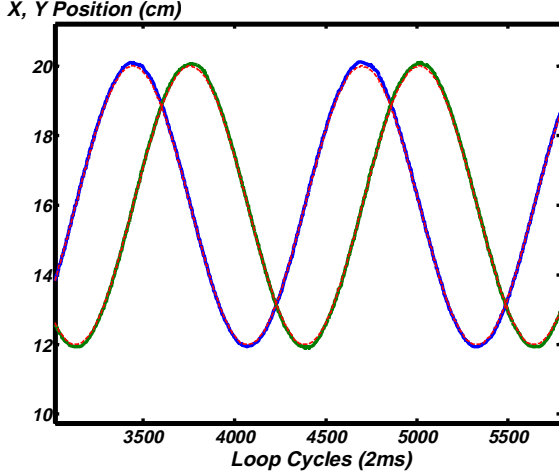


**Figure 2** The object position response of the system (blue— x position and green y-position) to a cicular motion control (dashed red).

**Sensor Fusion** – The problem of sensor fusion involves converting the high-dimensional output of many sensors,  $\mathbf{y}$ , into a low-dimensional state representation,  $\mathbf{x}^*$  within the control system loop time without losing relevant information. In general, this process can be accomplished by least squares fitting of the data (an optimization problem). An estimate of the system state,  $\mathbf{x}^*$ , found from the observations  $\mathbf{y}$  can be given as a solution to the minimization problem

$$\min_{\mathbf{x}} (\mathbf{y} - h(\mathbf{x}))^T W(\mathbf{x})(\mathbf{y} - h(\mathbf{x})) \quad (2)$$

where  $W(\mathbf{x})$  is a positive definite weighting matrix that may be a function of the system state. Note that there often may be more than one such solution. Finding the minimum solutions,  $\mathbf{x}^*$  to Eq. (2) entail the *sensor fusion* process and effectively convert the sensor data into a state estimation for both linear and nonlinear systems.

**Actuator Allocation** – The estimated state  $\mathbf{x}^*$  is used to determine the actuation  $\mathbf{u}$  that generates a desired change  $g(\mathbf{x}^*, \mathbf{u})$  in the system state given by

$$g(\mathbf{x}^*, \mathbf{u}) = -K(\mathbf{x}^*) \quad (3)$$

where  $K(\mathbf{x}^*)$  is a user-specified control law. Thus, the rhs of Eq. (3) is known and assuming  $g(\mathbf{x}^*, \mathbf{u})$  is known, one must solve for  $\mathbf{u}$ . In large-scale systems there are many possible actuator values  $\mathbf{u}$  that approximately solve this equation. One would like to use the additional degrees of freedom to attain other desirable goals. In particular, the force allocation problem can be solved as a *constrained optimization problem*, [Fromherz & Jackson] where the objective function represents desirable secondary goals and the constraints denote the required forces and torques. This optimization problem is solved at each control time step in order to determine which jets should be activated. Hence, the applied actuation  $\mathbf{u}^*$  is determined by the solution to the optimization problem

$$\begin{aligned} \min_{\mathbf{u}} d(\mathbf{u}) \\ \text{s.t. } g(\mathbf{x}^*, \mathbf{u}) = -K(\mathbf{x}^*) \end{aligned} \quad (4)$$

where the objective function  $d(\mathbf{u})$  expresses the desirability of various possible actuations  $\mathbf{u}$ . The solution to this constrained optimization problem, actuator allocation, converts the low-dimensional ( $\mathbf{x}^*$ ) into the high-dimensional actuation vector  $\mathbf{u}$ . The control solution is restricted to the next time step to reduce the necessary computation compared with usual MPC control.

**System Self-Identification** – Finally, the above procedures assume that  $f(\mathbf{x})$ ,  $g(\mathbf{x}, \mathbf{u})$  and  $h(\mathbf{x})$  are known functions.  $f(\mathbf{x})$  is low-dimensional and can be determined using standard system identification methods. For the present work, we assume that  $h(\mathbf{x})$  is determined in the standard way; future work will address finding  $h(\mathbf{x})$  by comparing individual sensor readings against the group (sensor self-identification). The function  $g(\mathbf{x}, \mathbf{u})$  can be determined in the following manner. Suppose that the system is held to a time averaged steady state position,  $\mathbf{x}_{st}$ . Then from Eq. (1), the aggregate time-averaged actuator effect on the state of the system,  $\langle g(\mathbf{x}_{st}, \mathbf{u}_{st}) \rangle$  due to an externally applied actuation is given by

$$\langle g(\mathbf{x}_{st}, \mathbf{u}_{st}) \rangle = -\langle f(\mathbf{x}_{st}) \rangle - \langle f_{ext}(\mathbf{x}_{st}) \rangle \quad (5)$$

Once the aggregate time averaged actuation  $\langle g(\mathbf{x}_{st}, \mathbf{u}_{st}) \rangle$  is known, a single actuator  $u_i$  can be held on and then held off while the time averaged actuation can be measured in both cases. Taking differences yields

$$\begin{aligned} \langle g(\mathbf{x}_{st}, \mathbf{u}_{st}) \rangle_{on} - \langle g(\mathbf{x}_{st}, \mathbf{u}_{st}) \rangle_{off} = \\ -\langle f(\mathbf{x}_{st}) \rangle_{on} + \langle f(\mathbf{x}_{st}) \rangle_{off} \end{aligned} \quad (6)$$

It should be noted that  $\mathbf{x}_{st}$  and  $\mathbf{u}_{st}$  change between the cases where the single jet is held on or off. The important point is that for large-scale systems, where the combined force of many actuators is much larger than that due to a single actuator, the steady-state time-averaged values  $\mathbf{x}_{st}$  and  $\mathbf{u}_{st}$  do not change significantly if a single actuator is held on or off. The dependence of  $g(\mathbf{x}_{st}, \mathbf{u}_{st})$  on the system steady state ( $\mathbf{x}_{st}$ ) due to a single jet can then be approximately determined by measuring the difference between the time-averaged actuation with one or more actuators on and then off. The above relations will be used to analyze the air-jet system.

### 3. Brief Description of Hardware

The system hardware consists of the following components. Further details may be found in [Berlin *et al.* 2000; Biegelsen *et al.* 2000]. The object moving system consists of a 12”x12” array of 1,152 air jets that obliquely impinge on the object to impart lateral momentum to flat objects such as paper using viscous drag. The jets are split

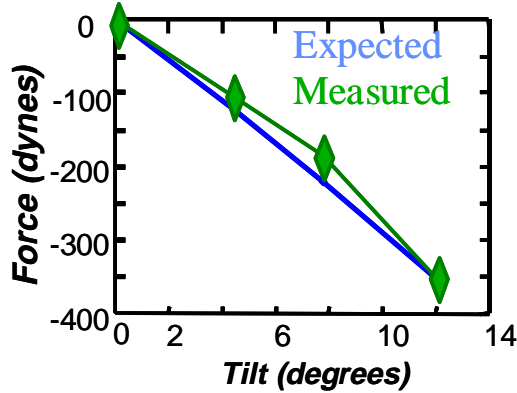


**Figure 3** Expected component of gravitational force (blue) with measured force (green) using Eq. (5)

between a top and bottom half and are actuated in pairs, a jet on the top is paired with a mirrored jet on the bottom. The air jets are canted in one of four perpendicular directions from the normal, thereby providing viscous drag forces in  $+x$ ,  $-x$ ,  $+y$ , or  $-y$  directions. Each jet can be individually actuated using electrostatic valves fabricated from printed circuit board based MEMS technology. The response times of the valves is roughly 1.5 ms opening time and 1.2 ms closing time. The actuation system therefore consists of 576 binary forces applied in one of four directions. Actuation of suitable combinations of the various directions results in application of in-plane forces and torques about the out-of-plane direction. Twenty-five CMOS linear image sensors, each of which consists of 1280 individual grayscale sensors, perform objection position sensing. These sensor arrays are dumped within 0.3 ms in order to determine the paper position and angle about the  $z$ -axis. The desired paper state ( $x$ ,  $y$  position and angle about the  $z$ -axis) is obtained from either a joy-stick or preprogrammed trajectory from a file. The real-time control computations are performed in a 40 MHz Analog Devices Sharc DSP. Logging, monitoring, display, and control setup are performed by a host PC. We found this to be an ideal system to identify and solve control problems for large-scale systems.

## 4. Control System

The implemented control system consists of the usual components, but some control operations that are trivial in small-scale systems dominate the control computations for large-scale systems (Fig. 1). In particular, for large-scale systems, points in the control loop that require large dimensional transformations between high and low dimensions are of critical importance. For the present system sensor fusion and actuation allocation are such critical steps.

### 4.1 Sensor Fusion

In the present case, the output of 30,000 sensors must be condensed to yield the three state variables,  $x$  position,  $y$  position, and angle of the sheet of paper as well as the three corresponding velocities. The sensor fusion is accomplished using the following procedure.

An important step in large-scale sensor fusion is discarding sensor outputs that do not contain useful information. Accordingly, the output of each of the 25 sensors is clocked out into a comparator that triggers when the sensor outputs cross a threshold when changing from light to dark or from dark to light. The crossing point for the edge of the paper on each sensor is determined from that time, i.e., the pixel at which the transition occurs. Thus, the gray values of 30,000 pixels are reduced to about 50 crossing points for each loop time and these 50 points are transferred to the controlling DSP. This immense data reduction step is equivalent to setting many elements of  $W(x^*)$  to zero in Eq. (2) using hardware and is critical to insure that the higher-level processing is not overwhelmed with non-essential information. This step is equivalent to edge location in a visual field often used in computer vision.

The array of crossing points is then fit to a model of the paper [Bern and Goldberg, 2000]: a rectangle of known dimensions or a series of two pairs of parallel orthogonal lines. The fitting procedure involves first computing a center of mass of the crossing points and then ordering the crossing points according to angle around the center of mass. The slope between neighboring pairs of angle ordered points is computed in order to group the points into appropriate sides of the rectangle. A least squares fit is performed to find the best fitting candidate rectangles. The least squares fit most closely matching the expected position that is based on the velocity and previous position and consistent with the previous size estimate of the rectangle, is selected as the current paper position. Low pass filtered derivatives of the current position provide the position and angular velocity estimates. We achieved the goal of a position accuracy of the sensor resolution/ $\sqrt{\text{Number edge of sensors}}=127\mu\text{m}/5=25\mu\text{m}$  rms error, a result indicating effective sensor fusion.

### 4.2 Control

For this large-scale system, the current estimated lateral and angular positions and velocities,  $\mathbf{x}^*$ , are compared with the desired positions and velocities,  $\mathbf{x}_d$ , and used to compute forces and torques using a standard first-order lead controller given by  $K(\mathbf{x}^*) = \mathbf{K}_m(\mathbf{x}_d - \mathbf{x}^*) = [F_x/m, F_y/m, T_z/I_z]^T$  where  $\mathbf{K}_m$ , a standard gain matrix. The  $x$ ,  $y$  and  $\theta$  axes are assumed to be decoupled. The mass and moment of inertia of the paper are  $m$  and  $I_z$  respectively.

### 4.3 Actuator Allocation

Consider the problem of generating an optimal allocation  $\mathbf{u}^*$  for the air jets in order to produce the desired forces and torques  $[F_x/m, F_y/m, T_z/I_z]^T = g(\mathbf{x}, \mathbf{u})$  using Eq. (4). One could attempt to solve the problem directly for  $\mathbf{u}$  given a suitable objective function  $d(\mathbf{u})$ . Because the forces are discrete, the NP problem for optimal allocation can be found using exhaustive search within the loop time only for systems where the number of jets is on the order of ten or less. Instead, for large numbers of jets, we developed a hierarchical solution to Eq. (4) that produces near-optimal results [Fromherz & Jackson]. In this hierarchical solution, actuators are grouped into modules. Eq. (4) is solved for allocation each module. Eq. (4) is then solved to find the allocation for even smaller submodules until the force for actual jets is assigned. In particular, assume that there are  $N$  modules with jets in  $x$  and  $y$  directions. Each module is located at a position  $(x_i, y_i)$  ( $i = 1, \dots, N$ ) relative to the sheet's center of mass, i.e., the module effective jet applies its force at position  $(x_i, y_i)$ . These quantities are therefore dependent on the estimated object position  $\mathbf{x}^*$ . Consider the objective that minimizes the force applied to the paper. Hence, a possible constrained optimization problem capturing such desired behavior is

$$\min_{u_{xi}, u_{yi}} d(\mathbf{u}) = \frac{1}{2} \sum_{i=1}^N \frac{u_{xi}^2}{w_{xi}^2} + \frac{1}{2} \sum_{i=1}^N \frac{u_{yi}^2}{w_{yi}^2} \quad (7)$$

subject to

$$g(\mathbf{x}, \mathbf{u}) = \begin{bmatrix} F_x/m \\ F_y/m \\ T_z/I_z \end{bmatrix} = \begin{bmatrix} \sum_{i=1}^N u_{xi}/m \\ \sum_{i=1}^N u_{yi}/m \\ \sum_{i=1}^N (x_i u_{yi} - y_i u_{xi})/I_z \end{bmatrix} \quad (8)$$

where  $\mathbf{u}_i = (u_{xi} \ u_{yi})$  are the allocated  $x$  and  $y$  forces for module jet  $i$ , and  $\mathbf{w}_i = (w_{xi} \ w_{yi})$  are the weighting factors for each module's contribution to the  $x$  and  $y$  force, respectively. A large weighting factor causes the module to assume a greater role in meeting the constraints for forces and torque and a smaller role in minimizing the objective function. Analytic optimal continuous solutions  $\mathbf{u}_i^* = (u_{xi}^* \ u_{yi}^*)$  for Eqs. (7) and (8) can be found. These solutions for each module in turn can be substituted for  $F_x, F_y, T_z=0$  in Eqs. (7) and (8) and solved for submodule force allocations. Finally when the submodules contain a sufficiently small number of jets, an optimal allocation within a submodule can be found using table lookup or exhaustive search.

As shown in Fromherz & Jackson, this hierarchical solution to the actuation allocation optimization problem of Eq. (4) performs well. For small numbers of actuators ( $<10$ ), direct optimization provides the optimal solution. As the numbers of actuators approaches a continuum limit, the hierarchical allocation approaches

the continuous solution. For intermediate numbers of jets, the hierarchical solution method provides a near-optimal solution. The solution time increases logarithmically with time, which makes this hierarchical approach appropriate for large-scale systems. Specifically, for 100 jets the hierarchical solution is  $10^4$  times faster while the *rms* error is about  $10^{1.8}$  times larger than the optimal search. The *rms* allocation error is 0.08 jets, an acceptably small error.

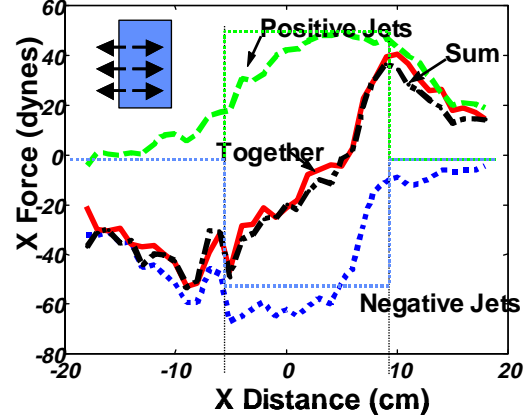


**Figure 4** X Force from columns (see inset figure) of  $+x$ -directed jets (thick green),  $-x$ -directed jets (thick blue), simultaneous (red) and sum (black). Thin lines indicate assumed profiles.

## 5. Results

The performance of the control system in controlling the position of sheets of paper is shown in the following figures. The tracking error following a circular motion is shown in Fig. 2. The *rms* error is 116  $\mu\text{m}$  for the position error direction (blue and green) compared with the desired (red dashed lines). The error is primarily due to low net actuator authority and saturation at the ends of the travel. For hold to position, the *rms* error is about 23  $\mu\text{m}$  and 0.48 mrad for the angle.

The control performance that has been achieved without much tuning is the following. The open-loop crossover frequency is about 15 Hz. The stability margins are 45 degrees for the phase margin and 10 db for the gain margin. The settling time (10%) for a large step response is 150 msec. These numbers are dominated by the fact that the actuators are often in saturation. The sensor fusion step is accomplished in about 0.34 msec, the control is computed in 0.01 ms, and the actuation allocation takes about 0.86 msec to complete. Optimizing data structures and data access operations in the prototype system can easily reduce this time.

## 6. Self Identification

System identification and self-identification was accomplished as described in Section 4. The system was run open loop to measure the response of the system to full actuation and drift. The velocity increased linearly with actuation and remained constant when the actuation is turn off. This behavior verifies that the system can be described as a simple  $1/s^2$  system without observable viscous drag. The results of the open loop response yielded that  $f(x)=Ax$ , where  $A$  is the usual matrix for friction-free object motion. By measuring the acceleration, the aggregate force was computed to be 16.7 dynes per jet with later modifications to air-jet fabrication yielding 33 dynes per jet.

Closing the feedback loop and holding the object to a constant position, an external force was applied to the object by tilting the air table. The total actuation signal was averaged over time and compared to the projection of the known gravitational force along the channel (application of Eq. (5)). For the case of frictionless object motion, a linear system  $g(x,u)=B(x)u$ , and binary actuation of a single jet ( $u_j=\{0,1\}$ ), Eq. (6) reduces to

$$B_{ij}(x_{st}) \approx - \left\langle \sum_l B_{il}(x_{st}) u_l \right\rangle_{u_{j,on}} + \left\langle \sum_l B_{il}(x_{st}) u_l \right\rangle_{u_{j,off}} \quad Eq. (9)$$

The results are shown in Fig. 3. The agreement between expected and measured forces indicates that the aggregate force is accurately determined. The next step in system identification is to use Eq. (6) or (9) to determine the dependence of the actuation on the held state of the

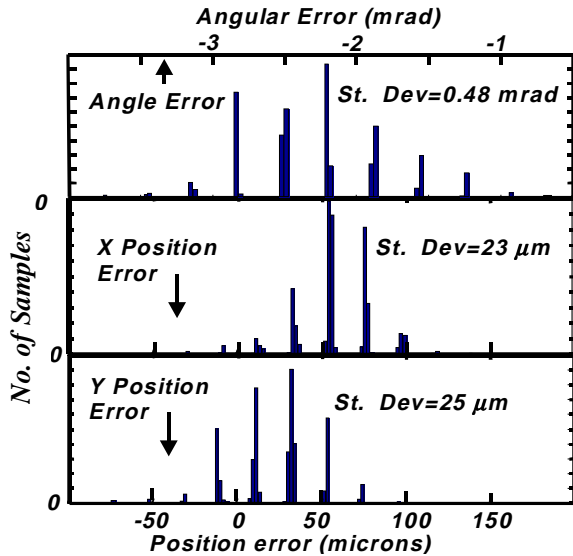


**Figure 6** Histogram of position and angle errors during hold to position

object. For columns of y jets facing away from each other (inset in Fig. 4), the difference in the hold force with the columns of jets held off and the columns of jets held on was determined as a function of the object position. The results are shown in Fig. 4.

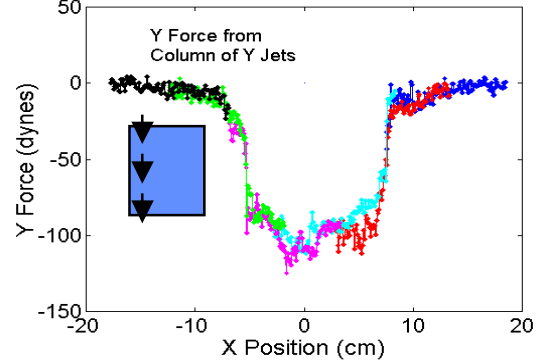


**Figure 5** Force due to a column of -y directed jets(see inset). The different colors indicate data from different portions of the array but same relative position

The thick green dashed line indicates the force due to three jets as the held object position is scanned with respect to the jets. The thin green line indicates the assumed profile, i.e., the jet only provides force when the jet is under the object and zero otherwise. The force arising from the negative jets is depicted with the blue line. The combined force from the columns of jets operating simultaneously (red) overlaps in great detail with the sum of the positive and negative jet curves verifying the linear superposition of the force despite the interaction of the air jets. Thus, the force of each jet can be determined and used to refine the combined jet force estimate. The new combined jet force can be used to refine the estimate of individual jets.

Fig. 5 shows the force from a column of y jets on a sheet of paper as the paper position is scanned relative to the air-jet column and was computed using self-identification (Eq. (9)). The different colors represent different data sets as the column position is changed relative to the scan range of the paper. The data show that the detailed structure is not noise but rather fine features of the dependence of the actuation force on the state of the paper (its position). Note that, due to air-jet spreading, the force extends beyond the paper by 3-4 cm (wings beyond the sharp drop in Fig. 5).

Fig. 6 shows the position and angle errors for a hold to position. Because the force and time are discrete (a minimum position step size  $\sim 25 \mu\text{m}$ ) and the sensor is size is  $127 \mu\text{m}$ , the possible positions and angles are discrete. The results indicate that our control is typically within a step size of the hold position even though the sensor size is about 5 times larger. Note that there is no integral term so there is a dc offset.

## 7. Conclusions

Large-scale systems require new methods for real time, constrained actuator allocation, sensor fusion, and system identification. In this paper, we have presented an integrated approach, which was implemented for an air-jet object transport system. We have found that, in both sensor and actuator aspects, hierarchical solutions based on constrained optimization generate acceptable solutions within the time constraints.

For sensor fusion, data compression and consolidation is important to reduce the information transfer load. Sensor data that contribute noise or uncertainty but little positional information must be effectively eliminated by weighting (or throwing out useless information). Using constrained optimization in hierarchical stages proved to be a powerful way of generating near-optimal actuator allocation within the time constraints. We were able to determine the position to 1/6 of the individual sensor reading for about 15 sensor crossing points—a result indicating effective sensor fusion. Eq. (4) or its instantiation for air jets in Eqs. (7) and (8) is used for different hierarchical levels, where a solution at one level is incorporated as a constraint or target for the next-lower level, and efficiently generates near optimal solutions for actuation. The hierarchical constrained optimization yields a good compromise between computational speed and accuracy. Moreover, constrained optimization leads to robust and desirable solutions to both sensor fusion and actuator allocation.

Finally, having many sensors and actuators enables one to perform system-ID by a successive approximation process of self-identification. First, the aggregate behavior of the actuators is determined. Then the individual actuators work against the group in order to determine specific details of the individual actuators. The individual actuator response can then be grouped to determine a better estimate of the aggregate actuator response. A similar procedure (not discussed here) may be invoked for individual sensor calibration against the group of sensors. These results apply to most systems consisting of large numbers of actuators and sensors.

## References

- Allgöwer F., T. A. Badgwell, S. J. Qin, J. B. Rawlings and S. J. Wright, 1999, “Nonlinear Model Predictive Control”, in P. M. Frank (Ed.), *Advances in Control*, pp. 391-449.
- Bemporad A, F.D. Torrisi and M. Morari Performance, “Analysis of Piecewise Linear Systems and Model Predictive Control System”, *Proc. 39th IEEE Conference on Decision and Control*, Sydney, Australia, 2000.
- Bequette, B. W. 1991. “Nonlinear control of chemical processes: A review”, *Ind. Eng. Chem. Res.* **30**: 1391-1413.
- Berlin, A.; Biegelsen, D.; Cheung, P.; Fromherz, M.; Goldberg, D.; Jackson, W. B.; Preas, B.; Reich, J. and Swartz, L.E.

”Motion Control of Planar Objects Using Large-area Arrays of MEMS-like Distributed Manipulators”. In: *Micromechanics '2000*, 2000.

Bern, M. and Goldberg, D. and "Sensor Fusion in an Air-jet Paper Mover", to be published.

Biegelsen, D.; Berlin, A.; Cheung, P.; Fromherz, M.; Goldberg, D.; Jackson, W. B.; Preas, B.; Reich, J. and Swartz, L.E. "Airjet Paper Mover: An Example of Meso-scale MEMS", in: Eric Peeters, Oliver Paul (eds.), *SPIE, Micromachined Devices and Components VI*, Santa Clara, CA, Invited Paper, vol. 4176, Sep. 2000, pp. 122-129.

Fromherz, M. and Jackson, W. "Force Allocation in a Large-scale Air-jet Table", to be published.

Rawlings, J. B. Muske, K. R. 1993. "Stability of constrained receding horizon control", *IEEE Trans. Auto. Cont.* 38(10): 1512-1516.